BIOCHEMISTRY
including biophysical chemistry & molecular biology

Article

pubs.acs.org/biochemistry

Binding of 3,4,5,6-Tetrahydroxyazepanes to the Acid-β-glucosidase Active Site: Implications for Pharmacological Chaperone Design for Gaucher Disease

Susan D. Orwig,[†] Yun Lei Tan,[‡] Neil P. Grimster,[‡] Zhanqian Yu,[‡] Evan T. Powers,[‡] Jeffery W. Kelly,[‡] and Raquel L. Lieberman*[,†]

[†]School of Chemistry and Biochemistry, Georgia Institute of Technology, Atlanta, Georgia 30332, United States

[‡]Skaggs Institute for Chemical Biology, Departments of Chemistry and Molecular and Experimental Medicine, The Scripps Research Institute, La Jolla, California 92037, United States

Supporting Information

ABSTRACT: Pharmacologic chaperoning is a therapeutic strategy being developed to improve the cellular folding and trafficking defects associated with Gaucher disease, a lysosomal storage disorder caused by point mutations in the gene encoding acid-β-glucosidase (GCase). In this approach, small molecules bind to and stabilize mutant folded or nearly folded GCase in the endoplasmic reticulum (ER), increasing the concentration of folded, functional GCase trafficked to the lysosome where the mutant enzyme can hydrolyze the accumulated substrate. To date, the pharmacologic chaperone (PC) candidates that have been investigated largely have been active site-directed inhibitors of GCase, usually containing five- or six-membered rings, such as modified azasugars. Here we show that a seven-membered, nitrogen-containing heterocycle (3,4,5,6-tetrahydroxyazepane) scaffold is also promising for generating PCs for GCase. Crystal structures reveal that the core azepane stabilizes GCase in a variation of its proposed active conformation, whereas binding of an analogue with an N-linked hydroxyethyl tail stabilizes GCase in a conformation in which the active site is covered, also utilizing a loop conformation not seen previously. Although both compounds preferentially stabilize GCase to thermal denaturation at pH 7.4, reflective of the pH in the ER, only the core azepane, which is a mid-micromolar competitive inhibitor, elicits a modest increase in enzyme activity for the neuronopathic G202R and the non-neuronopathic N370S mutant GCase in an intact cell assay. Our results emphasize the importance of the conformational variability of the GCase active site in the design of competitive inhibitors as PCs for Gaucher disease.

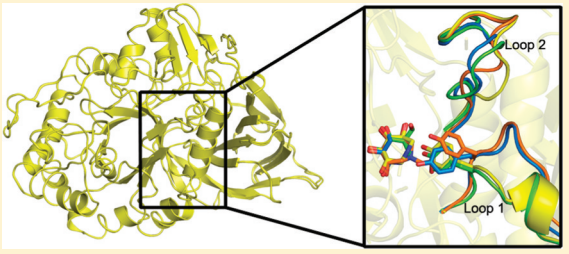

Gaucher disease (GD), the most common lysosomal storage disorder (LSD), is caused by inherited point mutations in acid-β-glucosidase (GCase), a lysosomal enzyme that hydrolyzes glucosylceramide (GlcCer) (Figure 1) as its main substrate.[1] Disease-associated GCase mutations are not localized to its active site.[2,3] Rather, variants exhibit defects in protein stability[4] and cellular trafficking defects[5] leading to endoplasmic reticulum (ER) retention[6] and/or ER-associated degradation,[7,8] and accumulation of GlcCer and related substrates in the lysosome. Clinically, organomegalies, a weakened skeleton, and, in severe cases, central nervous system complications are observed.[1,9] Enzyme replacement[10] and substrate reduction therapy (SRT)[11−13] are successful if rather expensive[14] treatments for non-neuronopathic (type 1) GD, but there is no treatment for neuronopathic GD, the most prevalent form of the disease worldwide.[15] The emerging pharmacologic chaperone (PC) therapeutic strategy proposes to use a small molecule to stabilize the endogenous mutant folded GCase enzyme in the ER to allow more mutant GCase to engage its trafficking receptor, LIMP-2.[16] An increase in the concentration of active GCase in the lysosome would then turn over the substrate and mitigate clinical symptoms. PCs hold promise, particularly for the treatment of neuronopathic GD variants, because small molecules can cross the blood−brain barrier[10] and also should be attractive in terms of cost to help overcome worldwide accessibility issues.

The desirable properties of ideal PCs include high binding selectivity and affinity for the folded or near-folded mutant enzymes, which increase the competent enzyme pool for trafficking and turnover. Somewhat paradoxically, the best PC candidates for GCase are noncovalent active-site-directed inhibitors, but because GCase has several close relatives in vivo, selective binding among closely related enzymes has been an ongoing challenge.[17,18] Non-active site-directed binders for GCase are still in the early stages of development.[19,20] One class of active site-directed PC molecules for GCase is the deoxynojirimycins [DNJs (Figure 1)], first identified for SRT as an inhibitor of glucosylceramide synthase.[17] *N*-Butyldeoxynojir-

Received: October 24, 2011
Revised: November 1, 2011
Published: November 2, 2011

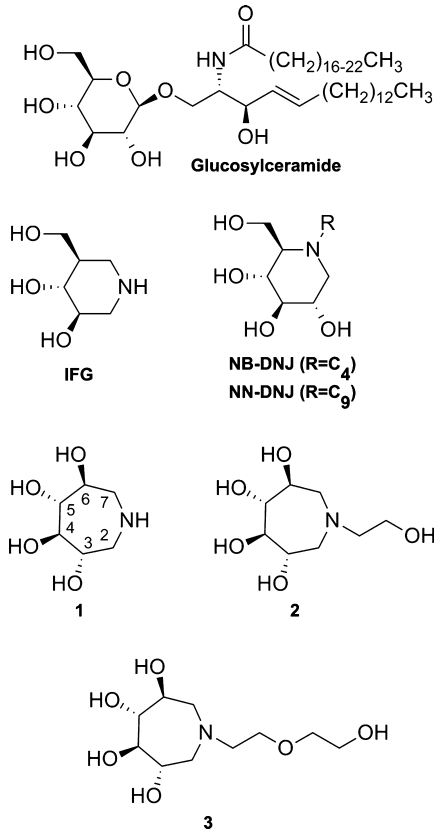

Figure 1. Chemical structures of the natural GCase substrate, GlcCer, representative azasugars investigated as pharmacologic chaperones, IFG, NB- and NN-DNJs, and azepane compounds **1**−**3** described in this study.

imycin (NB-DNJ) exhibited very weak chaperoning of mutant GCase in cell culture,[21,22] whereas a related analogue, *N*-(*n*-nonyl)deoxynojirimycin (NN-DNJ), with a 10-fold lower half-maximal inhibitory concentration (IC_{50}), was capable of chaperoning one of the two most prevalent GCase variants, namely, the non-neuronopathic N370S variant, but not the neuronopathic L444P variant.[22] Issues of enzyme selectivity[18] and toxicity[23] of DNJ analogues linger, and these compounds have not been tested in human clinical trials.[24] Other compounds such as cyclic-fused nojirimycin hybrids,[25−28] iminoxylitols,[29] N-substituted *δ*-lactams,[30] imino D-glucitols,[22,31] *N*-octyl-*β*-valienamine (NOV),[32,33] aminocyclitols,[34−36] the non-sugar Ambroxyl, an FDA-approved drug for an unrelated ailment,[8,37] and quinazoline analogues[38] are under investigation as PCs for GD but are not yet progressing through clinical trials. Until recently, the leading clinical candidate had been isofagomine (Figure 1; IFG, Plicera), an active site-directed[39] and selective[40] iminosugar product analogue, with a low nanomolar IC_{50}. IFG chaperones N370S[41] and L444P[40] mutant GCase in cell culture. Unfortunately, although the drug was well tolerated, clinical trials were halted after phase 2 trials in 2009 because of the lack of a therapeutic effect,[42] which might be due to large doses or off-target effects, among many other possibilities.[43]

Optimism for the PC approach remains high, but the example of IFG illustrates the complexities in the design, development, and clinical application of a therapeutic GCase pharmacologic chaperone. In spite of a body of work detailing the synthesis of candidate PCs for mutant GCase and their characterization in vitro, in patient-derived cell lines, and in some cases in animal models, the characteristics that make a PC a good clinical candidate remain poorly understood. We therefore have been seeking new PC scaffolds for GCase. In this work, we synthesized and characterized three GCase active site-directed 3,4,5,6-tetrahydroxyazepane inhibitors [**1**−**3** (Figure 1)] that exhibit IC_{50} values in the low millimolar to micromolar range, a reasonable starting point for structure-based design. While the synthesis of polyhydroxylated seven-membered ring structures has been known for more than 40 years,[44] these analogues have only recently been explored as inhibitors of commercially available[45−51] or human[52,53] glycosidases. Prior studies have not included GCase, and no analogues previously synthesized contain alkyl ether substructures attached to the endocyclic nitrogen like the inhibitors described herein. Our structural results demonstrate significant plasticity in the active site of GCase and this can be exploited for the design of active site-directed inhibitors as PCs for GD.

EXPERIMENTAL PROCEDURES

Synthesis of Compounds 1−3. *(1R,1′R)-1,1′-[(4R,5R)-2,2-Dimethyl-1,3-dioxolane-4,5-diyl]bis(ethane-1,2-diol) (**S-1**).* 2,2′-Dimethoxypropane (300 mL) was charged to a 1 L round-bottom flask. D-Mannitol (20 g, 0.11 mol) and pyridinium *p*-toluenesulfonate (1 mol %, 0.27 g, 2.0 mmol) were added, and the suspension was stirred at reflux. After 18 h, the solution was allowed to cool to room temperature and concentrated under reduced pressure. The residue was dissolved in ethyl acetate (300 mL) and washed with water (2 × 100 mL) and brine (100 mL). The organic layer was taken, dried over $MgSO_4$, filtered, and evaporated under reduced pressure. The resultant white solid was charged to a 1 L round-bottom flask. Acetic acid (210 mL) and water (90 mL) were added, and the suspension was stirred at 40 °C. After 2 h, the mixture was concentrated under reduced pressure. The residue was suspended in acetone (100 mL) and stirred at room temperature. After 1 h, the mixture was filtered and the filtrate concentrated under reduced pressure to yield **S-1** as a white solid (17.1 g, 70%): ^{1}H NMR (300 MHz, $CDCl_3$) *δ* 4.17−4.23 (m, 2H), 3.90−4.05 (m, 2H), 3.70−3.77 (m, 4H), 1.45 (s, 6H); LC−MS *m*/*z* 245.2 $[M + Na]^+$, calculated for $C_9H_{18}NaO_6^+$ 245.1. Data are consistent with the literature.[54]

*(1R,1′R)-[(4S,5S)-2,2-Dimethyl-1,3-dioxolane-4,5-diyl]bis-{2-[(tert-butyldimethylsilyl)oxy]ethane-1,1-diyl} Bis(4-methylbenzenesulfonate) (**S-2**).* **S-1** (7.5 g, 33.8 mmol) was charged to a 500 mL round-bottom flask under a nitrogen atmosphere. Anhydrous DMF (200 mL), imidazole (7.0 g, 100 mmol), and DMAP (0.16 g, 1.3 mmol) were added, and the mixture was stirred at 0 °C. After 10 min, TBSCl (10.1 g, 68.0 mmol) was added portionwise and the solution was allowed to warm to room temperature. After 18 h, the reaction mixture was diluted with an ether/hexane mixture (1:1, 500 mL), washed with water (3 × 100 mL), dried over $MgSO_4$, and concentrated under reduced pressure. Purification by flash column chromatography (silica, 9:1 hexane/ethyl acetate) afforded a colorless oil (8.0 g, 52%). A sample (6.82 g, 15.15 mmol) was charged to a 500 mL round-bottom flask. Anhydrous DCM (200 mL), DMAP (7.39 g, 60.5 mmol), and tosyl chloride were added, and the mixture was stirred at room temperature. After 18 h, the mixture was diluted with ethyl acetate (200 mL) and washed with water (100 mL), aqueous HCl (1 M, 100 mL), saturated aqueous $NaHCO_3$ (100 mL), and brine (100 mL). The organic layer was taken, dried over $MgSO_4$, filtered, and

concentrated under reduced pressure to afford **S-2** (10.0 g, 87%) as a white solid: ^{1}H NMR (300 MHz, $CDCl_3$) δ 7.81 (d, J = 8.4 Hz, 4H), 7.29 (d, J = 8.4 Hz, 4H), 4.68−4.72 (m, 2H), 4.36−4.40 (m, 2H), 3.83 (dd, J = 11.6, 4.6 Hz, 2H), 3.74 (dd, J = 11.6, 5.1 Hz, 2H), 2.43 (s, 6H), 1.14 (s, 6H), 0.83 (s, 18H), 0.1 (s, 12 H); LC−MS m/z 781.4 $[M + Na]^+$, calculated for $C_{35}H_{58}NaO_{10}S_2Si_2^+$ 781.3.

*(4R,5R)-2,2-Dimethyl-4,5-di[(S)-oxiran-2-yl]-1,3-dioxolane (**S-3**).* **S-2** (10.0 g, 13.2 mmol) was charged to a 500 mL round-bottom flask. THF (250 mL) and TBAF (1 M in THF, 29.0 mL, 29.0 mmol) were added, and the mixture was stirred at room temperature. After 2 h, the mixture was concentrated under reduced pressure, and the residue was dissolved in ether (100 mL) and washed with saturated aqueous $MgSO_4$ (3 × 100 mL), dried over $MgSO_4$, filtered, and concentrated under reduced pressure. The residue was dissolved in anhydrous THF (120 mL), sealed under a nitrogen atmosphere, and cooled to 0 °C. Sodium hydride (60% dispersion in mineral oil, 2.11 g, 52.7 mmol) was added portionwise. After 1 h, the reaction was quenched with an ice/water mixture (50 mL) and the mixture extracted with ether (3 × 20 mL). The organic layers were combined, dried over $MgSO_4$, filtered, and concentrated under reduced pressure. Purification by flash column chromatography (silica, 8:2 hexane/ethyl acetate) afforded **S-3** (1.5 g, 60%) as a white solid: ^{1}H NMR (300 MHz, $CDCl_3$) δ 3.86 (dd, J = 3.2, 1.6 Hz, 2H), 3.04−3.10 (m, 2H), 2.85 (dd, J = 5.2, 4.1 Hz, 2H), 2.74 (2H, J = 5.2, 2.6 Hz, 2H), 1.41 (s, 6H); LC−MS m/z 209.0 $[M + Na]^+$, calculated for $C_9H_{14}NaO_4^+$ 209.0. Data are consistent with the literature.[55]

*(3S,4R,5R,6S)-3,4,5,6-Tetrahydroxyazepan-1-ium Chloride (**1**).* **S-3** (120 mg, 0.64 mmol) was charged to a 5 mL round-bottom flask. Water (2 mL) and benzylamine (freshly distilled, 69 mg, 70 μL, 0.64 mmol) were added, and the mixture was stirred at 95 °C. After 2 h, the mixture was cooled to room temperature and concentrated under reduced pressure. Purification by flash chromatography (silica, 1:1 ethyl acetate/hexane) yielded a white solid, which was charged to a 10 mL round-bottom flask. Methanol (5 mL), palladium on carbon (10%, 60 mg), and ammonium formate (122 mg, 1.9 mmol) were added, and the mixture was stirred at 70 °C. After 2 h, the mixture was cooled to room temperature, and 1-heptene (1.86 g, 2.66 mL, 19.0 mmol) was charged to the vessel. After being stirred at room temperature for 1 h, the mixture was filtered through Celite and evaporated under reduced pressure. The residue was dissolved in methanol (5 mL), and methanolic HCl (1 M, 5 mL, 5 mmol) was added. The mixture was stirred at room temperature. After 1 h, the mixture was evaporated under reduced pressure to yield **1** as a gummy colorless solid (100 mg, 76% from **S-3**): ^{1}H NMR (300 MHz, D_2O) δ 4.06−4.18 (m, 2H), 3.69−3.76 (m, 2H), 3.34−3.44 (m, 2H), 3.18−3.30 (m, 2H); LC−MS m/z 164.3 $[M + H]^+$, calculated for $C_6H_{14}NO_4^+$ 164.1. Data are consistent with the literature.[55]

*(3S,4R,5R,6S)-3,4,5,6-Tetrahydroxy-1-(2-hydroxyethyl)-azepan-1-ium Chloride (**2**).* **S-3** (120 mg, 0.64 mmol) was charged to a 5 mL round-bottom flask. Water (2 mL) and ethanolamine (39 mg, 39 μL, 0.64 mmol) were added, and the mixture was stirred at 95 °C. After 2 h, the mixture was cooled to room temperature and concentrated under reduced pressure. The residue was dissolved in methanol (5 mL); methanolic HCl (1 M, 5 mL, 5 mmol) was added, and the mixture was stirred at room temperature. After 1 h, the mixture was evaporated under reduced pressure to yield **2** as a gummy yellow solid (144 mg, 93%): ^{1}H NMR (300 MHz, D_2O) δ 4.07−4.24 (m, 2H), 3.87−4.01 (m, 2H), 3.61−3.77 (m, 4H), 3.44−3.58 (m, 4H); LC−MS m/z 208.2 $[M + H]^+$, calculated for $C_8H_{18}NO_4^+$ 208.1.

*(3S,4R,5R,6S)-3,4,5,6-Tetrahydroxy-1-[2-(2-hydroxyethoxy)ethyl]azepan-1-ium Chloride (**3**).* **S-3** (120 mg, 0.64 mmol) was charged to a 5 mL round-bottom flask. Water (2 mL) and 2-(2-aminoethoxy)ethanol (67 mg, 64 μL, 0.64 mmol) were added, and the mixture was stirred at 95 °C. After 2 h, the mixture was cooled to room temperature and concentrated under reduced pressure. The residue was dissolved in methanol (5 mL); methanolic HCl (1 M, 5 mL, 5 mmol) was added, and the mixture was stirred at room temperature. After 1 h, the mixture was concentrated under reduced pressure to yield **3** as a gummy yellow solid (174 mg, 95%): ^{1}H NMR (300 MHz, D_2O) δ 4.10−4.23 (m, 2H), 3.92−3.99 (m, 2H), 3.61−3.80 (m, 4H), 3.34−3.57 (m, 8H); LC−MS m/z 208.1 $[M + H]^+$, calculated for $C_8H_{18}NO_4^+$ 208.1.

In Vitro GCase Inhibition Assay. Fifteen nanograms of Cerezyme (Genzyme Corp.) was mixed with McIlvaine buffer [0.1 M citrate and 0.2 M phosphate (pH 5.4)], 0.1% Triton X-100, 0.25% taurochloric acid, and various concentrations of **1**, **2**, or **3** on ice. A stock of 300 mM 4-methylumbelliferyl-β-glucopyranoside [4MU-β-Glc (Sigma)] was freshly prepared in dimethyl sulfoxide (DMSO) and added to the Cerezyme/inhibitor mixture at a final concentration of 3 mM. The mixture was then transferred into a microplate (Grenier), and the microplate was sealed and incubated at 37 °C for 30 min. An equal volume of 0.4 M glycine and 0.4 M NaOH was added to each well to quench the reaction. The release of 4-methylumbelliferone (4MU) was measured by fluorescence (excitation at 360 nm with a 40 nm slit width, emission at 460 nm with a 40 nm slit width) on a BioTek microplate reader. Each mixture was set up in triplicate per plate, averaged, and background subtracted. Each plate was repeated in triplicate per inhibitor, and the averaged, normalized data were plotted versus drug concentration and fitted to a log(inhibitor) versus response-variable slope curve in GraphPad Prism to estimate the IC_{50}. To investigate the effect of incubation time of the premixed inhibitor and enzyme, the Cerezyme/**2** mixture was incubated at 4 °C for 16 h. 4MU-β-Glc was then added and the assay conducted as described above. An inhibition assay with IFG (Toronto Research Chemicals) was also conducted as a positive control with a result similar to that previously published.[39]

Thermal Stability Assay for GCase. Cerezyme was resuspended in 0.1 M citrate and 0.2 M phosphate, adjusted to pH 5.2 or 7.2, and the protein concentration was determined via a Bradford assay.[56] A working stock of 10 μM Cerezyme was prepared by dilution in the appropriate buffer. Reaction mixtures (30 μL) were prepared at room temperature by dilution of Cerezyme in water (1:10) along with various concentrations of inhibitor (0−10 mM), also prepared in water. This resulted in final buffer concentrations of 0.01 M citrate, 0.02 M phosphate (pH 5.2 or 7.2), and 1 μM protein. Finally, Sypro Orange (Invitrogen, supplied as a 5000× solution in DMSO) was diluted in water and then added to each reaction mixture with a final concentration of 5×. Each mixture was delivered to 96-well optical plates (Applied Biosystems) before they were sealed with optical film. Fluorescence data were acquired on an Applied Biosciences Step-One Plus RT-PCR instrument equipped with a fixed excitation wavelength (480 nm) and a ROX emission filter (610 nm). Melts were

Table 1. Data collection and refinement statistics

	3RIL (1)	3RIK (2)
	Data Statistics	
space group	$P2_1$	$P2_1$
cll dimensions		
a, *b*, *c* (Å)	109.2, 91.4, 152.7	108.0, 91.6, 152.2
α, β, γ (deg)	90.0, 110.95, 90.0	90.0, 110.70, 90.0
resolution (Å)[a]	44.5−2.4 (2.49−2.40)	46.5−2.5 (2.55−2.48)
R_{sym}[a]	10.5 (35.7)	12.2 (47.8)
% > 3σ[a]	62.9 (38.3)	64.6 (40.7)
completeness (%)[a]	96.3 (76.5)	94.3 (72.3)
redundancy	2.6	2.9
	Refinement Statistics	
resolution (Å)	44.5−2.4	47−2.5
no. of reflections	100648 (5857)	88126 (4973)
R_{work}/R_{free}[b]	20.8/24.9	18.1/23.4
no. of molecules		
protein molecules in the asymmetric unit	4	4
protein residues	1988	1988
N-acetylglucosamine (NAG)	4	4
sulfate anion (SO_4^{2-})	7	7
chaperone	4	2
water	1254	702
B factor (Å^2)		
protein	23.6	26.6
NAG	29.7	50.4
SO_4^{2-}	60.8	38.1
chaperone	38.2	32.9
water	27.6	40.0
root-mean-square deviation		
bond lengths (Å)	0.006	0.013
bond angles (deg)	1.089	1.466

[a]Data for the highest-resolution shell are given in parentheses. [b]Five percent of the reflections were selected for R_{free}.

conducted from 25 to 95 °C at a rate of 1 °C/min. Collected data were baseline subtracted, trimmed to include both the boundaries and the transition of interest, and subjected to Boltzmann sigmoid analysis as described previously.[57]

Intact Cell GCase Activity Assay. Primary skin fibroblast cultures established from Gaucher patients homozygous for the G202R GCase (c.721G > A) mutation were kindly provided by Dr. K.-P. Zimmer, Children's Hospital of the University of Munster. The heterozygous Gaucher fibroblasts containing the N370S/V394L GC mutation (GM01607) were obtained from the Coriell Cell Repositories (Camden, NJ). Fibroblasts were grown in minimal essential medium with Earle's salts (supplemented with 10% heat-inactivated fetal bovine serum and 1% glutamine Pen-Strep at 37 °C in 5% CO_2). Cell culture media were obtained from Gibco (Grand Island, NY). Briefly, cells were plated into 96-well plates (100 μL/well). After cell attachment, the medium was replaced with fresh medium containing candidate PCs and incubated at 37 °C for 3 days. The medium was removed, and cell monolayers were washed with Dulbecco's phosphate-buffered saline. The assay was started by the addition of 50 μL of 2.5 mM 4MU-β-Glc in 0.2 M acetate buffer (pH 4.0) to each well, followed by incubation at 37 °C for 1−4 h. The extent of unspecific nonlysosomal GC activity was evaluated by adding CBE (Toronto Research Chemicals) to control wells. The reaction was stopped by the addition of 150 μL of 0.2 M glycine buffer (pH 10.8). Liberated 4MU was measured (excitation at 365 nm, emission at 445 nm) with a Molecular Devices SpectraMax Gemini fluorescence plate reader. Small molecules were assayed in at least triplicate at each concentration, and on three different days. Cells appeared intact when viewed under a light microscope. The data reported were normalized to the enzyme activity of cells of the same type treated with vehicle control (H_2O) and expressed as a percentage of wild-type (WT) enzyme activity.

Crystallization, Data Collection, Structure Determination, and Refinement. Cerezyme was partially deglycosylated with N-glycosidase F (Promega) and concentrated to 3 mg/mL in 0.02% sodium azide, 10 mM citrate buffer (pH 5.5), and 7% (v/v) ethanol. Crystals of GCase were grown by vapor diffusion at room temperature using a cocktail composed of 11−12% PEG 3350, 0.18−0.205 M ammonium sulfate, and 0.1 M acetate buffer (pH 4.6). Crystals of **1** and **2** were generated by soaking crystals in the reservoir solution supplemented with 1 mM inhibitor for 5 min and 5 days, respectively. Crystals were protected with 20% ethylene glycol and cryocooled in liquid N_2. Data were collected at the Southeast Regional Collaborative Access Team (SER-CAT) Beamlines at the Advanced Photon Source at Argonne National Laboratories (Darien, IL). Data sets were indexed and scaled using HKL2000,[58] and structures were determined by rigid body refinement in REFMAC5[59] utilizing the asymmetric unit of just the GCase polypeptide [four copies of GCase in the asymmetric unit of Protein Data Bank (PDB) entry 2NSX] as the initial model. Compounds were identified by significant (>3σ) $F_o - F_c$ difference Fourier density in the active site after initial rigid body refinement (Figure 3). All four active site

copies in the asymmetric unit were occupied with **1**, whereas with **2**, like for IFG,[39] only two of the four active site copies had bound ligand. Restrained refinement was performed against the highest resolution of the data with REFMAC5[59] and model rebuilding with Coot.[60] Models for **1** and **2** were generated using PRODRG[61] and figures generated using PyMOL.[62] For both structures, ≥99% of the residues lie in the most favored and additionally allowed regions of the Ramachandran plot. Crystallographic statistics are listed in Table 1, and coordinates have been deposited as PDB entries 3RIL (**1**) and 3RIK (**2**).

RESULTS AND DISCUSSION

Inhibitor Design and Synthesis. To extend the previously studied five-membered ring scaffolds and six-membered ring glucose-derived PCs,[4,9,22,63] three seven-membered 3,4,5,6-tetrahydroxyazepane iminosugar analogues [**1**–**3** (Figure 1)] were synthesized as potential GCase inhibitors and PCs by procedures slightly modified from those reported in the literature[55] (see Schemes 1–3 and Experimental Procedures).

Scheme 1. Synthesis of Diepoxide S-3

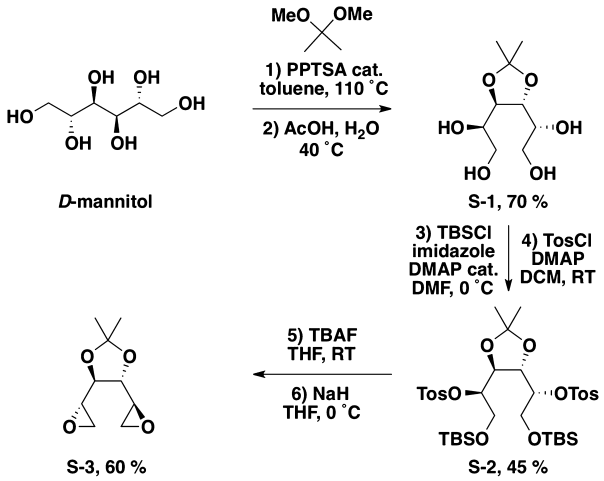

Scheme 2. Synthesis of Tetrahydroxyazepane 1

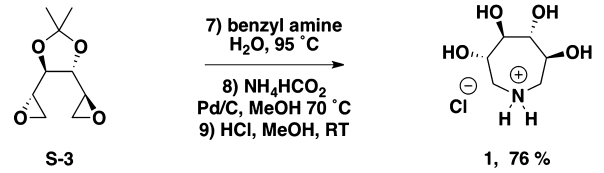

Scheme 3. Synthesis of Tetrahydroxyazepanes 2 and 3

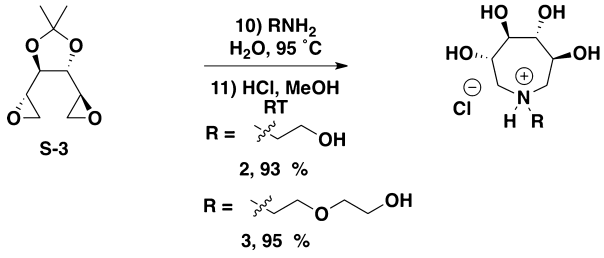

We included an endocyclic nitrogen because, depending on their binding orientation, protonated iminosugars and azasugars can mimic the glycosidase transition state.[64] In addition, the increased number of sites that can be functionalized can be exploited in future design efforts to tune the hydrogen bonding network to select against unwanted inhibition of other glucosidases, a known problem.[18] Finally, instead of the alkyl chains used previously, alkyl ether tails were installed to assist in discriminating between anomeric carbon configurations,[65] to reduce the lipophilicity of the candidate PC, to provide a better match with the polarity of the ceramide component of the substrate, and/or to decrease the cytotoxicity reported for related compounds.[17]

Inhibition Profiles. The inhibitory activities of compounds **1**–**3** toward GCase were determined by competition against the fluorogenic substrate 4MU-β-Glc.[66] Compound **1** exhibited the strongest competitive inhibition, with an IC_{50} of 146 μM (Figure 2a), comparable to that of DNJ (IC_{50} = 240 μM) and

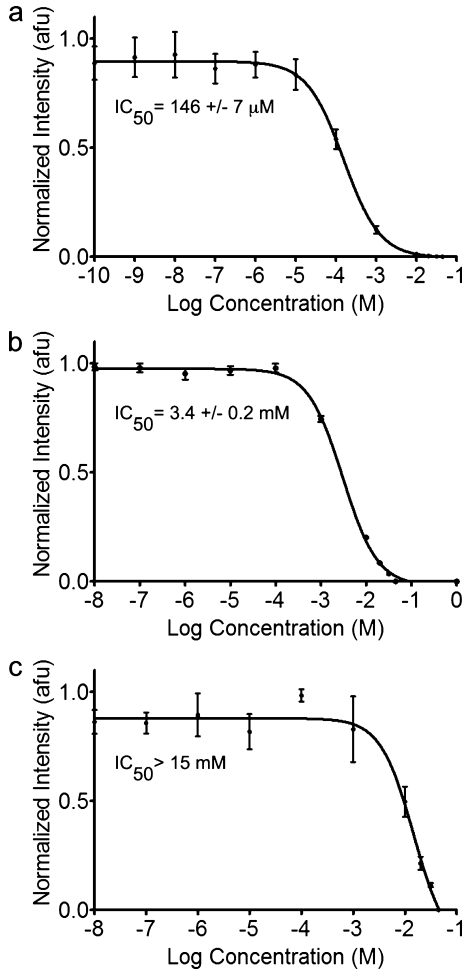

Figure 2. (a–c) Competitive inhibition curves for **1**–**3**, respectively, toward GCase. Inset are IC_{50} values. Error bars indicate the standard deviation.

NB-DNJ (IC_{50} = 270 μM)[67] but 10-fold weaker than that of NN-DNJ[22] and 250-fold weaker than that of IFG.[39] In contrast, compounds **2** and **3** exhibited weaker IC_{50} values of 3.4 and >15 mM, respectively (Figure 2b,c). To address the possibility of slow binding kinetics, GCase was preincubated with **2** for 16 h prior to the addition of substrate. No change in the IC_{50} value was observed, suggesting that the on rate is not slow (data not shown).

Stabilization to Thermal Denaturation. Because active-site-directed inhibitors are likely to stabilize GCase against

dx.doi.org/10.1021/bi201619z | Biochemistry 2011, 50, 10647–10657

Table 2. Stabilization of GCase with Inhibitors at Acidic and Neutral pH

		1		2		3		IFG	
	[inhibitor] (mM)	T_m (°C)	ΔT_m	T_m (°C)	ΔT_m	T_m (°C)	ΔT_m	T_m (°C)	ΔT_m
pH 5.2		55.8 ± 0.0[a]							
	0.5	56.4 ± 0.0	0.6	55.9 ± 0.1	0.3	56.1 ± 0.0	0.3	68.0 ± 0.2	12.2
	1	56.6 ± 0.0	0.8	56.0 ± 0.0	0.3	56.1 ± 0.1	0.2	68.9 ± 0.3	13.0
	2	57.3 ± 0.1	1.5	56.7 ± 0.1	1.0	56.7 ± 0.1	0.8	69.7 ± 0.3	13.8
	5	58.4 ± 0.1	2.7	57.4 ± 0.1	1.7	57.2 ± 0.1	1.3	67.5 ± 0.3	11.6
	10	59.0 ± 0.1	3.2	57.4 ± 0.0	1.7	56.9 ± 0.0	1.0	63.7 ± 0.2	7.8
pH 7.2		47.1 ± 0.2[a]							
	0.5	48.5 ± 0.1	1.4	48.7 ± 0.1	1.7	50.7 ± 0.0	2.1	63.8 ± 0.3	16.9
	1	49.4 ± 0.1	2.3	49.3 ± 0.0	2.2	52.0 ± 0.1	3.3	65.4 ± 0.1	18.4
	2	49.9 ± 0.1	2.8	50.1 ± 0.1	3.1	52.6 ± 0.1	3.9	67.2 ± 0.2	20.2
	5	52.5 ± 0.1	5.4	52.1 ± 0.1	5.0	53.6 ± 0.1	5.0	70.3 ± 0.2	23.4
	10	54.6 ± 0.1	7.5	53.6 ± 0.1	6.5	54.5 ± 0.0	5.8	72.6 ± 0.2	25.7

[a]Mean T_m measured for GCase at the indicated pH value in the absence of inhibitor.

thermal denaturation, we measured the change in the stability of GCase in the presence of inhibitor by differential scanning fluorimetry (DSF). Melting temperatures (T_m) recorded for GCase using the low-volume and facile DSF method are within ~3 K of those reported by DSC[68] using similar enzyme and inhibitor concentrations, but with slightly different buffers. Comparison of the T_m values for GCase in the presence of 10 mM inhibitors reveals an only 1−3 K increase in stability at acidic pH and a larger (~6−7.5 K) increase at neutral pH (Table 2). Thus, while stabilization is modest compared to IFG (Table 2), all three compounds confer more stability to GCase at a neutral pH (reflective of the pH in the ER) than at the lower lysosomal pH, but stabilize GCase approximately to the same extent.

Structural Characterization. Crystal structures of **1** and **2** bound to wild-type GCase were determined to 2.4 and 2.5 Å resolution, respectively (Table 1), whereas a structure with **3**, also the weakest binder, could not be obtained. Suitable quantities of mutant GCase were not available for crystallization trials, but the PC is designed to stabilize the near-folded state of the enzyme. The stabilized native conformation is expected to be the same for the wild-type and GD-causing missense variants. The global structure of GCase remains unchanged by ligand binding, but adjustments are seen in the active site and surrounding loop regions. Below, we focus on the relevant active site (Figure 3), loop (Figures 4 and 5), and interior regions (Figure 5) of GCase affected by binding of **1** and **2** and compare the structures to previously determined GCase structures with well-studied candidate PCs bound,[69] namely, IFG[39] and two DNJs.[70]

In the GCase active site, bound **1** and **2** are held in place by a hydrogen bonding network (Figure 3a,b). In the case of **2**, which is bound in a distorted chair conformation, the hydroxyl substituents at positions 3 and 4 (see Figure 1) are equatorial and within hydrogen bonding distance of the side chains of Asp127, Trp179, Asn234, and Trp381 on GCase, whereas the 6-hydroxyl moiety, also equatorial, is not involved in any polar interactions (Figure 3a). The main distortions from the chair conformation appear at positions 1 and 2, which face Asn234 and Glu235, the residue implicated as the general acid/base in catalysis.[2,71] Notably, the hydroxyl substituent at position 2 is restrained by a hydrogen bonding interaction with Asn234 and, from below, the catalytic nucleophile Glu340.[72] Glu340 is also within hydrogen bonding distance of the endocyclic nitrogen and hydroxyethyl tail; all three interactions with the Glu340 carboxylate side chain are quite short (~2.7 Å). By comparison, binding of **1** in the GCase active site appears to be less conformationally constrained. Similar interactions engage the equatorial 3- and 4-hydroxyl groups of **1** in the GCase active site (Figure 3b). An additional interaction of the 6-hydroxyl group with Tyr313 is seen, and the 2-hydroxyl group appears to be less distorted, now within hydrogen bonding distance of Asn234 only. This change in interaction with the hydroxyl group at position 2 may be a result of the conformationally mobile endocyclic nitrogen, which is not involved in any interactions with GCase (Figure 3a,b). The resolution of this structure is insufficient to clarify the details of the occupancy of different puckered states of the ring. Interestingly, even though **2** is stabilized by more polar interactions than the less strained **1**, it is the weaker competitive inhibitor (see above).

The binding orientations of **1** and **2** are close to those found in NB-DNJ-bound and NN-DNJ-bound (Figure 3c) GCase.[70] First, neither our compounds nor the DNJs are hydrogen bonded to Glu235. This is in contrast to IFG-bound GCase (Figure 3d), where a likely deprotonated Glu235 stabilizes the IFG endocyclic amino group.[39] Second, the positions of the endocyclic nitrogens of **1**, **2**, NB-DNJ, and NN-DNJ are nearly superimposable and shifted compared to those of IFG-bound GCase. However, in the case of NB- and NN-DNJ, the endocyclic nitrogens are held in place by a water-mediated hydrogen bond to the hydyroxyl group of Tyr244; a corresponding water molecule was not resolved in either of our two structures. The preferential binding mode appears to derive from the interaction between the 3-hydroxyl group on the inhibitor and Asn234 common to the DNJs, **1**, and **2** (Figure 3), but not IFG. This observation could be exploited in future design to tune the product or transition-state-mimicking properties of the compound.

Notable differences in structure are observed in the active site loops [loop 1, residues 311−319; and loop 2, residues 342−354 (Figure 4)] upon comparison of the modes of binding of **1** (yellow) and **2** (orange) to each other and to previously reported GCase structures with bound IFG and glycerol (green and blue, respectively). The alterations, particularly in loop 1, reinforce the notion that the conformational flexibility of GCase beyond the site of catalysis is an important consideration in the design of active site binders as PCs. Although loop 2 (residues 342−354) is also shifted 3.2 Å from its position in the IFG-bound or glycerol-bound[39] GCase structures (Figure S1 of the Supporting Information), this

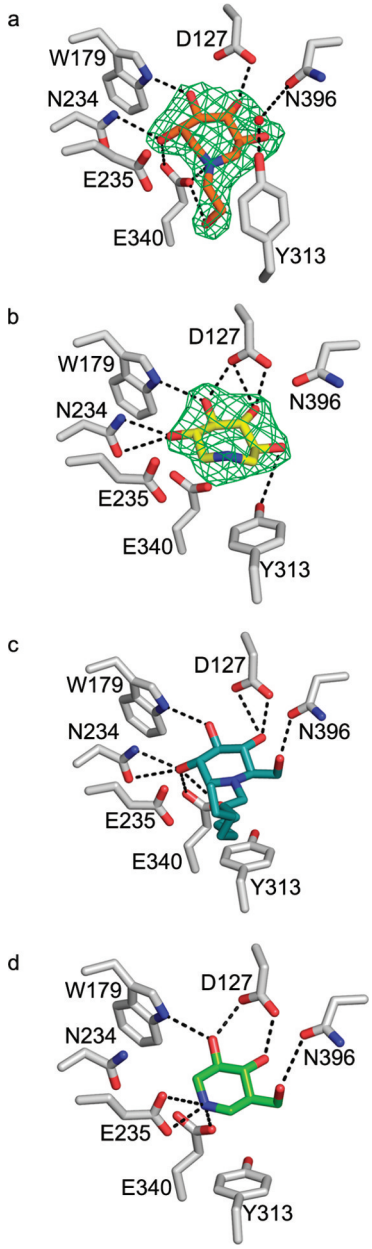

Figure 3. Ball-and-stick representation of the GCase active site upon compound binding: (a) **2**, (b) **1**, (c) NN-DNJ (PDB entry 2V3E), and (d) IFG (PDB entry 2NSX). Difference ($F_o - F_c$) electron density for **1** and **2** was calculated from the initial phasing solution using only protein coordinates and is contoured to 3σ. Hydrogen bonding interactions are represented by dashed lines and represent distances of 2.5−3.5 Å. Trp381 was omitted for the sake of clarity.

movement appears to be due to different crystal contacts used among the various GCase crystal forms. We observe the same orientation of loop 2 in apo GCase crystallized under the conditions used here for azepane inhibitor soaking (data not shown). By contrast, for loop 1, highly relevant changes due to ligand binding are observed. On the basis of the IFG-bound structure, helical loop 1 has been proposed to be the catalytically active form of GCase.[39] To date, this conformation has been observed only when a small molecule with reported chaperoning capabilities like those of the DNJ analogues[28,70] or IFG[39] is bound to the GCase active site; extended loop 1 has been seen with bound sulfate,[71] glycerol,[39] or the suicide

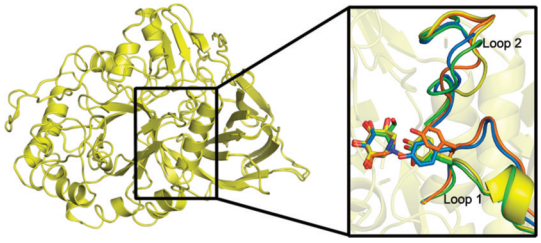

Figure 4. Superposition of **1**- and **2**-bound GCase structures and comparison of loops adjacent to the active site (inset). After binding, loop 1 adopts either a helical turn as seen for compound **1** (inset, yellow) and IFG (inset, green) or an extended loop conformation seen in compound **2** (inset, orange) and glycerol (inset, blue) bound structures. Changes in loop 2 are caused by crystal packing (see the text). Tyr313 is shown as ball-and-stick.

inhibitor conduritol β-epoxide (CBE),[73] and in the catalytically compromised N370S mutant GCase structure at neutral or acidic pH.[74]

At first glance, GCase adopts recognized loop 1 structures, namely, extended over the catalytic center when **2** binds and an α-helical arrangement (Figure 4 and Figure S2 of the Supporting Information) that exposes the active site when **1** is bound. However, each is distinct from conformations seen previously. For example, in other structures, the side chain of Tyr313 is within hydrogen bonding distance of the carboxylate of Glu235 when loop 1 is extended (not shown) but switches to interacting with Glu340 when loop 1 is helical (see Figure 5a). Although the expected helical loop 1 Tyr313−Glu340 interaction is seen when **1** is bound to GCase (Figure 5b), the interaction with Tyr313 for the extended loop 1 when **2** binds is not. The hydroxyethyl substituent on **2** replaces Tyr313 in hydrogen bonding interactions with Glu340 (Figure 5c), which leads to a new water-mediated interaction between Tyr313 and Asn396 (Figure 3a) that still caps the active site entrance. Second, in addition to changes near Tyr313 in the site of catalysis, helical turn-stabilizing interactions of loop 1 involving an interior helix of GCase have been altered when **1** is bound (Figure 5, bottom panels), leading to a more relaxed structure. For reference, as seen in the NB-DNJ, NN-DNJ, and IFG structures (see IFG in Figure 5a, bottom panel), Asp315 in the helical loop 1 forms a salt bridge with the guanidinium of Arg285 (omitted from Figure 5 for the sake of clarity) and is linked to Ser366 and Asn370 on the helix via bound water molecules (Figure 5a). Concurrently, the side chain of Trp312 interacts with the carbonyl backbone of Cys342, located on loop 2.[69] Unexpectedly, in our structure with **1** bound, the side chain of Trp312 is repositioned to form a new interaction with Ser366 instead of Cys342 (Figure 5b, bottom panel). This interaction has only been seen once before, in the low-pH structure of N370S GCase,[74] which retains ~30% catalytic activity in vitro[2] but where loop 1 is extended. The Trp312−Ser366 interaction serves to shift Asp315 away from Arg285 to a distance consistent with a hydrogen bonding interaction. This more relaxed loop 1 configuration observed with **1** bound may at least in part explain its weaker competitive inhibition compared to that with IFG or NN-DNJ.

Enhancement of Cellular Enzyme Activity. To evaluate **1**−**3** for PC activity, we next examined their abilities to enhance mutant GCase activity in an intact cell assay.[22] Patient-derived skin fibroblasts harboring either mutant G202R GCase (associated with neuronopathic type 2 GD) or mutant N370S/V394L GCase (associated with non-neuronopathic

dx.doi.org/10.1021/bi201619z | Biochemistry 2011, 50, 10647−10657

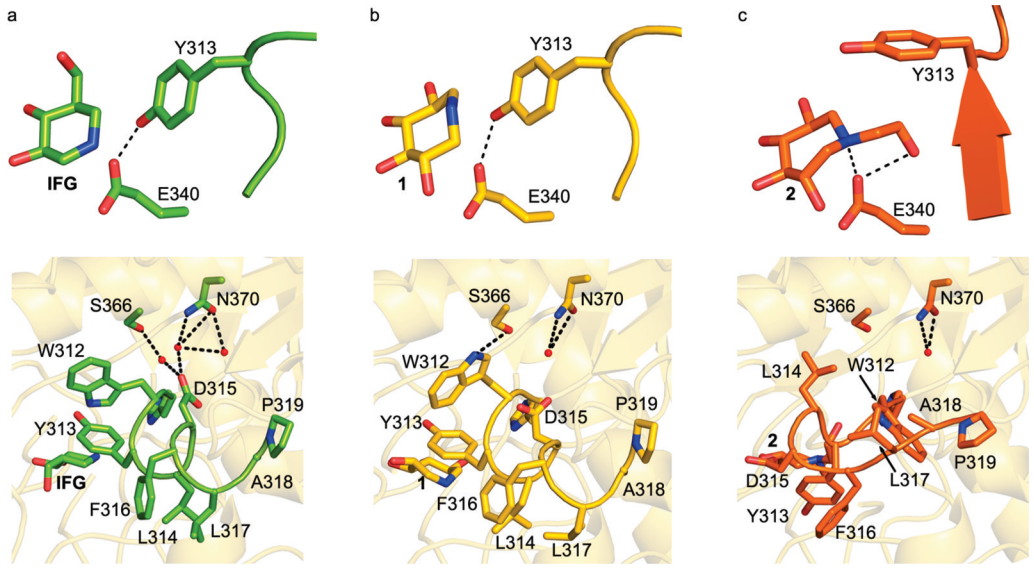

Figure 5. Comparison of loop 1 configurations: (a) IFG-, (b) **1**-, and (c) **2**-bound GCase. The top panels show the orientations of Tyr313 relative to Glu340. The bottom panels show the interactions of the loop with the interior GCase helix harboring Asn370. Hydrogen bonding interactions are represented by dashed lines.

type 1 GD) were incubated with compound **1**, **2**, or **3** for 3 days at varying concentrations. On the basis of cytotoxicity data from related compounds,[17,23] the upper limit tested was 100 μM. Compound **1** increased the cellular GCase activity of G202R fibroblasts by 20% at 100 μM, whereas **2** and **3** had no effect on activity in the concentration range tested (Figure 6a). A similar, but attenuated, result was obtained for N370S/V394L GCase fibroblasts. An ~15% increase in activity was observed for cells treated with 10 μM **1** (Figure 6b), a concentration lower than that required for a similar effect with G202R and comparable to the optimal concentration observed for NN-DNJ.[22] The maximal 20% activity enhancement for G202R GCase is intermediate between no enhancement exhibited by NB-DNJ and the 60−65% enhancement seen for NN-DNJ using the same enzyme variant and setup.[22] These activity enhancements are in the desired range of 10−15% of wild-type enzyme activity shown to reduce clinical manifestations in a related LSD[75] and thought to be a threshold of activity in the lysosome necessary to prevent GD symptoms.[76] Thus, the modest increase in activity, while not sufficient to claim that **1** is a bona fide PC candidate for GCase, suggests that the azepane ring system is a promising scaffold for future structure-based design efforts for the development of novel PCs for GCase.

CONCLUSIONS

In this study, we synthesized N-linked hydroxy alkyl and alkyl ether azepane inhibitors **1**−**3** as potential PCs for GCase. The active site of GCase readily accommodates the larger seven-membered azepane ring, but the enzyme is exquisitely sensitive to binding and can propagate binding-induced conformational changes as far away as ~13 Å from the binding site, within the interior of the enzyme. Compounds **1**−**3** stabilize GCase against thermal denaturation to approximately the same extent and preferentially at neutral versus acidic pH. However, only **1**, which exhibits an ~10-fold better competitive inhibition profile than **2** and **3**, exhibits any enhancement of enzyme activity in fibroblasts expressing G202R and N370S mutant GCase. Binding of **1** results in a helical arrangement of loop 1, albeit

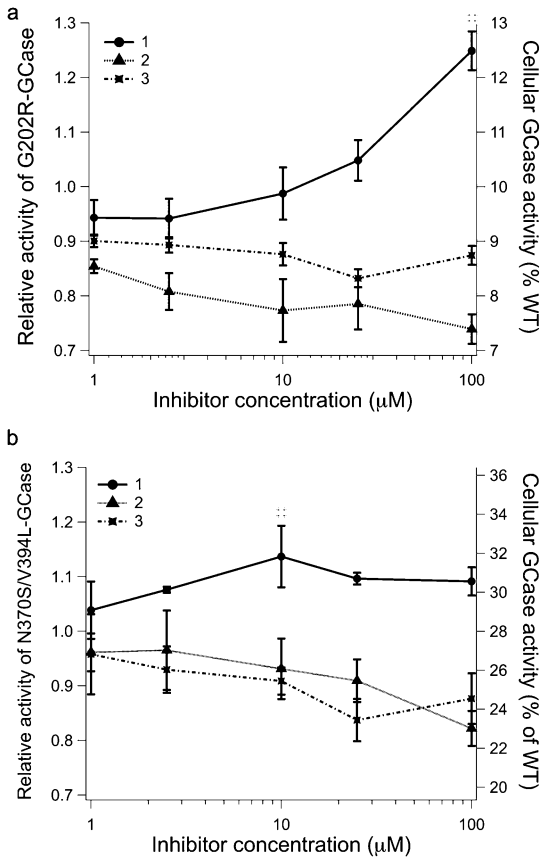

Figure 6. Effects of **1**−**3** on mutant GCase activity in intact patient-derived fibroblasts: G202R (a) and N370S/V394L (b). Enzyme activity is normalized to untreated cells, which were assigned a relative activity of 1. The right-hand axis is the residual activity of the mutant expressed as the percentage of WT GCase activity. Mean values for triplicate experiments are shown. Number signs denote $p < 0.05$.

one that is more relaxed than those observed previously for IFG and DNJs.[69] Notably, **2** generates a GCase loop conformation thought to be inactive, and this compound does not exhibit a

dx.doi.org/10.1021/bi201619z | *Biochemistry* 2011, 50, 10647−10657

favorable chaperoning profile in cells. In summary, a link is emerging between competitive inhibition of GCase in vitro and the conformation of loop 1 that exposes the GCase active site, with the ability to increase mutant GCase activity in cell culture. Thermal stabilization, a common feature of an inhibitor, is not a singular adequate predictor of cellular enzyme activity enhancement for GCase. The core azepane **1** appears to be a promising scaffold on which to build more potent competitive inhibitors as potential PCs. For example, inferred from a comparison of crystal structures, the introduction of a 6-hydroxymethyl substructure and removal of a 3-hydroxyl group, or the introduction of unsaturated bonds[25,26,28] into **1** may shift binding to better mimic the transition state or product and thereby generate a better competitive azepane inhibitor. It may also be possible to overcome some of the selectivity issues by taking advantage of the GCase active site plasticity, which may bind PC scaffolds that cannot be accommodated in related enzymes. Overall, we anticipate that biochemical and structural studies of potential PCs with corresponding enzyme structures will continue to provide valuable insight into priorities for inhibitor design that will lead to the identification of compounds worthy of detailed cellular trafficking and animal model studies and, ultimately, to a successful outcome of clinical trials for a therapeutic PC for GD.

■ ASSOCIATED CONTENT

Ⓢ Supporting Information

Figures S1 and S2. This material is available free of charge via the Internet at http://pubs.acs.org.

■ AUTHOR INFORMATION

Corresponding Author

*Address: 901 Atlantic Drive NW, Atlanta, GA 30332-0400. Phone: (404) 385-3663. Fax: (404) 894-2295. E-mail: raquel.lieberman@chemistry.gatech.edu.

Funding

This work was sponsored by National Institutes of Health Grant F32AG027647, the Blanchard Foundation, and the Pew Foundation (R.L.L.), and National Institutes of Health Grant R01DK075295 (J.W.K.). S.D.O. was supported in part by U.S. Department of Education Graduate Assistance in Areas of National Need Program P200A060188. Use of the APS was supported by the U.S. Department of Energy, Office of Science, Office of Basic Energy Sciences, under Contract W-31-109-Eng-38.

■ ABBREVIATIONS

GCase, acid-β-glucosidase; ER, endoplasmic reticulum; GD, Gaucher disease; NB-DNJ, *N*-butyldeoxynojirimycin; NN-DNJ, *N*-(*n*-nonyl)deoxynojirimycin; GlcCer, glucosylceramide; SRT, substrate replacement therapy; PC, pharmacologic chaperone; IFG, isofagomine; 4MU-β-Glc, 4-methylumbelliferyl-β-glucopyranoside; DSF, differential scanning fluorimetry; DSC, differential scanning calorimetry; T_m, melting temperature; LSD, lysosomal storage disorder.

■ REFERENCES

(1) Beutler, E., and Gelbart, T. (1996) Glucocerebrosidase (Gaucher disease). *Hum. Mutat. 8*, 207−213.

(2) Liou, B., Kazimierczuk, A., Zhang, M., Scott, C. R., Hegde, R. S., and Grabowski, G. A. (2006) Analyses of variant acid β-glucosidases: Effects of Gaucher disease mutations. *J. Biol. Chem. 281*, 4242−4253.

(3) Grace, M. E., Newman, K. M., Scheinker, V., Berg-Fussman, A., and Grabowski, G. A. (1994) Analysis of human acid β-glucosidase by site-directed mutagenesis and heterologous expression. *J. Biol. Chem. 269*, 2283−2291.

(4) Sawkar, A. R., Schmitz, M., Zimmer, K. P., Reczek, D., Edmunds, T., Balch, W. E., and Kelly, J. W. (2006) Chemical chaperones and permissive temperatures alter localization of Gaucher disease associated glucocerebrosidase variants. *ACS Chem. Biol. 1*, 235−251.

(5) Schmitz, M., Alfalah, M., Aerts, J. M., Naim, H. Y., and Zimmer, K. P. (2005) Impaired trafficking of mutants of lysosomal glucocerebrosidase in Gaucher's disease. *Int. J. Biochem. Cell Biol. 37*, 2310−2320.

(6) Zimmer, K. P., le Coutre, P., Aerts, H. M., Harzer, K., Fukuda, M., O'Brien, J. S., and Naim, H. Y. (1999) Intracellular transport of acid β-glucosidase and lysosome-associated membrane proteins is affected in Gaucher's disease (G202R mutation). *J. Pathol. 188*, 407−414.

(7) Ron, I., and Horowitz, M. (2005) ER retention and degradation as the molecular basis underlying Gaucher disease heterogeneity. *Hum. Mol. Genet. 14*, 2387−2398.

(8) Bendikov-Bar, I., Ron, I., Filocamo, M., and Horowitz, M. (2011) Characterization of the ERAD process of the L444P mutant glucocerebrosidase variant. *Blood Cells, Mol., Dis. 46*, 4−10.

(9) Yu, Z., Sawkar, A. R., and Kelly, J. W. (2007) Pharmacologic chaperoning as a strategy to treat Gaucher disease. *FEBS J. 274*, 4944−4950.

(10) Cox, T. M. (2010) Gaucher disease: Clinical profile and therapeutic developments. *Biologics 4*, 299−313.

(11) Lee, L., Abe, A., and Shayman, J. A. (1999) Improved inhibitors of glucosylceramide synthase. *J. Biol. Chem. 274*, 14662−14669.

(12) Lukina, E., Watman, N., Arreguin, E. A., Banikazemi, M., Dragosky, M., Iastrebner, M., Rosenbaum, H., Phillips, M., Pastores, G. M., Rosenthal, D. I., Kaper, M., Singh, T., Puga, A. C., Bonate, P. L., and Peterschmitt, M. J. (2010) A phase 2 study of eliglustat tartrate (Genz-112638), an oral substrate reduction therapy for Gaucher disease type 1. *Blood 116*, 893−899.

(13) Lukina, E., Watman, N., Arreguin, E. A., Dragosky, M., Iastrebner, M., Rosenbaum, H., Phillips, M., Pastores, G. M., Kamath, R. S., Rosenthal, D. I., Kaper, M., Singh, T., Puga, A. C., and Peterschmitt, M. J. (2010) Improvement in hematological, visceral, and skeletal manifestations of Gaucher disease type 1 with oral eliglustat tartrate (Genz-112638) treatment: 2-year results of a phase 2 study. *Blood 116*, 4095−4098.

(14) Wraith, J. E. (2006) Limitations of enzyme replacement therapy: Current and future. *J. Inherited Metab. Dis. 29*, 442−447.

(15) Michelakakis, H., Skardoutsou, A., Mathioudakis, J., Moraitou, M., Dimitriou, E., Voudris, C., and Karpathios, T. (2002) Early-onset severe neurological involvement and D409H homozygosity in Gaucher disease: Outcome of enzyme replacement therapy. *Blood Cells, Mol., Dis. 28*, 1−4.

(16) Reczek, D., Schwake, M., Schroder, J., Hughes, H., Blanz, J., Jin, X., Brondyk, W., Van Patten, S., Edmunds, T., and Saftig, P. (2007) LIMP-2 is a receptor for lysosomal mannose-6-phosphate-independent targeting of β-glucocerebrosidase. *Cell 131*, 770−783.

(17) Butters, T. D., van den Broek, L. A. G. M., Fleet, G. W. J., Krulle, T. M., Wormald, M. R., Dwek, R. A., and Platt, F. M. (2000) Molecular requirements of imino sugars for the selective control of N-linked glycosylation and glycosphingolipid biosynthesis. *Tetrahedron: Asymmetry 11*, 113−124.

(18) Mellor, H. R., Neville, D. C., Harvey, D. J., Platt, F. M., Dwek, R. A., and Butters, T. D. (2004) Cellular effects of deoxynojirimycin analogues: Inhibition of N-linked oligosaccharide processing and generation of free glucosylated oligosaccharides. *Biochem. J. 381*, 867−875.

(19) Landon, M. R., Lieberman, R. L., Hoang, Q. Q., Ju, S., Caaveiro, J. M., Orwig, S. D., Kozakov, D., Brenke, R., Chuang, G. Y., Beglov, D., Vajda, S., Petsko, G. A., and Ringe, D. (2009) Detection of ligand binding hot spots on protein surfaces via fragment-based methods: Application to DJ-1 and glucocerebrosidase. *J. Comput.-Aided Mol. Des. 23*, 491−500.

(20) Zheng, W., Padia, J., Urban, D. J., Jadhav, A., Goker-Alpan, O., Simeonov, A., Goldin, E., Auld, D., LaMarca, M. E., Inglese, J., Austin, C. P., and Sidransky, E. (2007) Three classes of glucocerebrosidase inhibitors identified by quantitative high-throughput screening are chaperone leads for Gaucher disease. *Proc. Natl. Acad. Sci. U.S.A. 104*, 13192−13197.
(21) Alfonso, P., Pampin, S., Estrada, J., Rodriguez-Rey, J. C., Giraldo, P., Sancho, J., and Pocovi, M. (2005) Miglustat (NB-DNJ) works as a chaperone for mutated acid β-glucosidase in cells transfected with several Gaucher disease mutations. *Blood Cells, Mol., Dis. 35*, 268−276.
(22) Sawkar, A. R., Cheng, W. C., Beutler, E., Wong, C. H., Balch, W. E., and Kelly, J. W. (2002) Chemical chaperones increase the cellular activity of N370S β-glucosidase: A therapeutic strategy for Gaucher disease. *Proc. Natl. Acad. Sci. U.S.A. 99*, 15428−15433.
(23) Chang, H. H., Asano, N., Ishii, S., Ichikawa, Y., and Fan, J. Q. (2006) Hydrophilic iminosugar active-site-specific chaperones increase residual glucocerebrosidase activity in fibroblasts from Gaucher patients. *FEBS J. 273*, 4082−4092.
(24) Sawkar, A. R., D'Haeze, W., and Kelly, J. W. (2006) Therapeutic strategies to ameliorate lysosomal storage disorders: A focus on Gaucher disease. *Cell. Mol. Life Sci. 63*, 1179−1192.
(25) Brumshtein, B., Aguilar-Moncayo, M., Garcia-Moreno, M. I., Ortiz Mellet, C., Garcia Fernandez, J. M., Silman, I., Shaaltiel, Y., Aviezer, D., Sussman, J. L., and Futerman, A. H. (2009) 6-Amino-6-deoxy-5,6-di-N-(N′-octyliminomethylidene)nojirimycin: Synthesis, biological evaluation, and crystal structure in complex with acid β-glucosidase. *ChemBioChem 10*, 1480−1485.
(26) Luan, Z., Higaki, K., Aguilar-Moncayo, M., Ninomiya, H., Ohno, K., Garcia-Moreno, M. I., Ortiz Mellet, C., Garcia Fernandez, J. M., and Suzuki, Y. (2009) Chaperone activity of bicyclic nojirimycin analogues for Gaucher mutations in comparison with N-(n-nonyl)deoxynojirimycin. *ChemBioChem 10*, 2780−2792.
(27) Aguilar-Moncayo, M., Garcia-Moreno, M. I., Trapero, A., Egido-Gabas, M., Llebaria, A., Fernandez, J. M., and Mellet, C. O. (2011) Bicyclic (galacto)nojirimycin analogues as glycosidase inhibitors: Effect of structural modifications in their pharmacological chaperone potential towards β-glucocerebrosidase. *Org. Biomol. Chem. 9*, 3698−3713.
(28) Brumshtein, B., Aguilar-Moncayo, M., Benito, J. M., Garcia Fernandez, J. M., Silman, I., Shaaltiel, Y., Aviezer, D., Sussman, J. L., Futerman, A. H., and Ortiz Mellet, C. (2011) Cyclodextrin-mediated crystallization of acid β-glucosidase in complex with amphiphilic bicyclic nojirimycin analogues. *Org. Biomol. Chem. 9*, 4160−4167.
(29) Oulaidi, F., Front-Deschamps, S., Gallienne, E., Lesellier, E., Ikeda, K., Asano, N., Compain, P., and Martin, O. R. (2011) Second-generation iminoxylitol-based pharmacological chaperones for the treatment of Gaucher disease. *ChemMedChem 6*, 353−361.
(30) Wang, G. N., Reinkensmeier, G., Zhang, S. W., Zhou, J., Zhang, L. R., Zhang, L. H., Butters, T. D., and Ye, X. S. (2009) Rational design and synthesis of highly potent pharmacological chaperones for treatment of N370S mutant Gaucher disease. *J. Med. Chem. 52*, 3146−3149.
(31) Yu, Z., Sawkar, A. R., Whalen, L. J., Wong, C. H., and Kelly, J. W. (2007) Isofagomine- and 2,5-anhydro-2,5-imino-D-glucitol-based glucocerebrosidase pharmacological chaperones for Gaucher disease intervention. *J. Med. Chem. 50*, 94−100.
(32) Lei, K., Ninomiya, H., Suzuki, M., Inoue, T., Sawa, M., Iida, M., Ida, H., Eto, Y., Ogawa, S., Ohno, K., and Suzuki, Y. (2007) Enzyme enhancement activity of N-octyl-β-valienamine on β-glucosidase mutants associated with Gaucher disease. *Biochim. Biophys. Acta 1772*, 587−596.
(33) Lin, H., Sugimoto, Y., Ohsaki, Y., Ninomiya, H., Oka, A., Taniguchi, M., Ida, H., Eto, Y., Ogawa, S., Matsuzaki, Y., Sawa, M., Inoue, T., Higaki, K., Nanba, E., Ohno, K., and Suzuki, Y. (2004) N-Octyl-β-valienamine up-regulates activity of F213I mutant β-glucosidase in cultured cells: A potential chemical chaperone therapy for Gaucher disease. *Biochim. Biophys. Acta 1689*, 219−228.
(34) Sanchez-Olle, G., Duque, J., Egido-Gabas, M., Casas, J., Lluch, M., Chabas, A., Grinberg, D., and Vilageliu, L. (2009) Promising results of the chaperone effect caused by imino sugars and aminocyclitol derivatives on mutant glucocerebrosidases causing Gaucher disease. *Blood Cells, Mol., Dis. 42*, 159−166.
(35) Diaz, L., Casas, J., Bujons, J., Llebaria, A., and Delgado, A. (2011) New glucocerebrosidase inhibitors by exploration of chemical diversity of N-substituted aminocyclitols using click chemistry and in situ screening. *J. Med. Chem. 54*, 2069−2079.
(36) Trapero, A., Alfonso, I., Butters, T. D., and Llebaria, A. (2011) Polyhydroxylated bicyclic isoureas and guanidines are potent glucocerebrosidase inhibitors and nanomolar enzyme activity enhancers in Gaucher cells. *J. Am. Chem. Soc. 133*, 5474−5484.
(37) Maegawa, G. H., Tropak, M. B., Buttner, J. D., Rigat, B. A., Fuller, M., Pandit, D., Tang, L., Kornhaber, G. J., Hamuro, Y., Clarke, J. T., and Mahuran, D. J. (2009) Identification and characterization of ambroxol as an enzyme enhancement agent for Gaucher disease. *J. Biol. Chem. 284*, 23502−23516.
(38) Marugan, J. J., Zheng, W., Motabar, O., Southall, N., Goldin, E., Westbroek, W., Stubblefield, B. K., Sidransky, E., Aungst, R. A., Lea, W. A., Simeonov, A., Leister, W., and Austin, C. P. (2011) Evaluation of quinazoline analogues as glucocerebrosidase inhibitors with chaperone activity. *J. Med. Chem. 54*, 1033−1058.
(39) Lieberman, R. L., Wustman, B. A., Huertas, P., Powe, A. C. Jr., Pine, C. W., Khanna, R., Schlossmacher, M. G., Ringe, D., and Petsko, G. A. (2007) Structure of acid β-glucosidase with pharmacological chaperone provides insight into Gaucher disease. *Nat. Chem. Biol. 3*, 101−107.
(40) Khanna, R., Benjamin, E. R., Pellegrino, L., Schilling, A., Rigat, B. A., Soska, R., Nafar, H., Ranes, B. E., Feng, J., Lun, Y., Powe, A. C., Palling, D. J., Wustman, B. A., Schiffmann, R., Mahuran, D. J., Lockhart, D. J., and Valenzano, K. J. (2010) The pharmacological chaperone isofagomine increases the activity of the Gaucher disease L444P mutant form of β-glucosidase. *FEBS J. 277*, 1618−1638.
(41) Steet, R. A., Chung, S., Wustman, B., Powe, A., Do, H., and Kornfeld, S. A. (2006) The iminosugar isofagomine increases the activity of N370S mutant acid β-glucosidase in Gaucher fibroblasts by several mechanisms. *Proc. Natl. Acad. Sci. U.S.A. 103*, 13813−13818.
(42) http://www.amicustherapeutics.com/clinicaltrials.
(43) Sun, Y., Ran, H., Liou, B., Quinn, B., Zamzow, M., Zhang, W., Bielawski, J., Kitatani, K., Setchell, K. D., Hannun, Y. A., and Grabowski, G. A. (2011) Isofagomine in vivo effects in a neuronopathic Gaucher disease mouse. *PLoS One 6*, e19037.
(44) Paulsen, H., and Todt, K. (1967) On monosaccharides with nitrogen-yielding seven membered rings. *Chem. Ber. 100*, 512−520.
(45) Painter, G. F., Eldridge, P. J., and Falshaw, A. (2004) Syntheses of tetrahydroxyazepanes from chiro-inositols and their evaluation as glycosidase inhibitors. *Bioorg. Med. Chem. 12*, 225−232.
(46) Qian, X., Moris-Varas, F., Fitzgerald, M. C., and Wong, C. H. (1996) C2-symmetrical tetrahydroxyazepanes as inhibitors of glycosidases and HIV/FIV proteases. *Bioorg. Med. Chem. 4*, 2055−2069.
(47) Moris-Varas, F., Qian, X., and Wong, C. H. (1996) Enzymatic/chemical synthesis and biological evaluation of seven-membered iminocyclitols. *J. Am. Chem. Soc. 118*, 7647−7652.
(48) Markad, S. D., Karanjule, N. S., Sharma, T., Sabharwal, S. G., and Dhavale, D. D. (2006) Polyhydroxylated homoazepanes and 1-deoxy-homonojirimycin analogues: Synthesis and glycosidase inhibition study. *Org. Biomol. Chem. 4*, 3675−3680.
(49) Li, H., Bleriot, Y., Chantereau, C., Mallet, J. M., Sollogoub, M., Zhang, Y., Rodriguez-Garcia, E., Vogel, P., Jimenez-Barbero, J., and Sinay, P. (2004) The first synthesis of substituted azepanes mimicking monosaccharides: A new class of potent glycosidase inhibitors. *Org. Biomol. Chem. 2*, 1492−1499.
(50) Shih, T. L., Liang, M. T., Wu, K. D., and Lin, C. H. (2011) Synthesis of polyhydroxy 7- and N-alkyl-azepanes as potent glycosidase inhibitors. *Carbohydr. Res. 346*, 183−190.
(51) Li, H., Liu, T., Zhang, Y., Favre, S., Bello, C., Vogel, P., Butters, T. D., Oikonomakos, N. G., Marrot, J., and Bleriot, Y. (2008) New synthetic seven-membered 1-azasugars displaying potent inhibition

towards glycosidases and glucosylceramide transferase. *ChemBioChem 9*, 253−260.
(52) Butters, T. D., Alonzi, D. S., Kukushkin, N. V., Ren, Y., and Bleriot, Y. (2009) Novel mannosidase inhibitors probe glycoprotein degradation pathways in cells. *Glycoconjugate J. 26*, 1109−1116.
(53) Marcelo, F., He, Y., Yuzwa, S. A., Nieto, L., Jimenez-Barbero, J., Sollogoub, M., Vocadlo, D. J., Davies, G. D., and Bleriot, Y. (2009) Molecular basis for inhibition of GH84 glycoside hydrolases by substituted azepanes: Conformational flexibility enables probing of substrate distortion. *J. Am. Chem. Soc. 131*, 5390−5392.
(54) Xiao, X., and Bai, D. (2001) An efficient and selective method for hydrolysis of acedonides. *Synlett 4*, 535−537.
(55) Lohray, B. B., Jayamma, Y., and Chatterjee, M. (1995) Unprecedented selectivity in the reaction of 1,2:5,6-dianhydro-3,4-O-isopropylidenehexitols with benzylamine: A practical synthesis of 3,4,5,6-tetrahydroxyazepanes. *J. Org. Chem. 60*, 5958−5960.
(56) Bradford, M. M. (1976) A rapid and sensitive method for the quantitation of microgram quantities of protein utilizing the principle of protein-dye binding. *Anal. Biochem. 72*, 248−254.
(57) Orwig, S. D., and Lieberman, R. L. (2011) Biophysical characterization of the olfactomedin domain of myocilin, an extracellular matrix protein implicated in inherited forms of glaucoma. *PLoS One 6*, e16347.
(58) Otwinowski, Z., and Minor, W. (1997) Processing of X-ray diffraction data collected in oscillation mode. *Methods Enzymol. 276*, 307−326.
(59) Collaborative Computational Project Number 4 (1994) The CCP4 Suite: Programs for Protein Crystallography. *Acta Crystallogr. D50*, 760.
(60) Emsley, P., Lohkamp, B., Scott, W. G., and Cowtan, K. (2010) Features and development of Coot. *Acta Crystallogr. D66*, 486−501.
(61) Schuttelkopf, A. W., and van Aalten, D. M. (2004) PRODRG: A tool for high-throughput crystallography of protein-ligand complexes. *Acta Crystallogr. D60*, 1355−1363.
(62) DeLano, W. L. (2002) *The PyMOL Molecular Graphics System*, DeLano Scientific, San Carlos, CA.
(63) Sawkar, A. R., Adamski-Werner, S. L., Cheng, W. C., Wong, C. H., Beutler, E., Zimmer, K. P., and Kelly, J. W. (2005) Gaucher disease-associated glucocerebrosidases show mutation-dependent chemical chaperoning profiles. *Chem. Biol. 12*, 1235−1244.
(64) Gloster, T. M., and Davies, G. J. (2010) Glycosidase inhibition: Assessing mimicry of the transition state. *Org. Biomol. Chem. 8*, 305−320.
(65) Aguilar-Moncayo, M., Gloster, T. M., Turkenburg, J. P., Garcia-Moreno, M. I., Ortiz Mellet, C., Davies, G. J., and Garcia Fernandez, J. M. (2009) Glycosidase inhibition by ring-modified castanospermine analogues: Tackling enzyme selectivity by inhibitor tailoring. *Org. Biomol. Chem. 7*, 2738−2747.
(66) Strasberg, P. M., and Lowden, J. A. (1982) The assay of glucocerebrosidase activity using the natural substrate. *Clin. Chim. Acta 118*, 9−20.
(67) Yu, L., Ikeda, K., Kato, A., Adachi, I., Godin, G., Compain, P., Martin, O., and Asano, N. (2006) α-1-C-Octyl-1-deoxynojirimycin as a pharmacological chaperone for Gaucher disease. *Bioorg. Med. Chem. 14*, 7736−7744.
(68) Lieberman, R. L., D'aquino, J. A., Ringe, D., and Petsko, G. A. (2009) The effects of pH and iminosugar pharmacological chaperones on lysosomal glycosidase structure and stability. *Biochemistry 48*, 4816−4827.
(69) Lieberman, R. L. (2011) A guided tour of the structural biology of Gaucher disease: Acid-β-glucosidase and saposin C. *Enzyme Res.*, in press.
(70) Brumshtein, B., Greenblatt, H. M., Butters, T. D., Shaaltiel, Y., Aviezer, D., Silman, I., Futerman, A. H., and Sussman, J. L. (2007) Crystal structures of complexes of N-butyl- and N-nonyl-deoxynojirimycin bound to acid β-glucosidase: Insights into the mechanism of chemical chaperone action in Gaucher disease. *J. Biol. Chem. 282*, 29052−29058.
(71) Dvir, H., Harel, M., McCarthy, A. A., Toker, L., Silman, I., Futerman, A. H., and Sussman, J. L. (2003) X-ray structure of human acid-β-glucosidase, the defective enzyme in Gaucher disease. *EMBO Rep. 4*, 704−709.
(72) Miao, S., McCarter, J. D., Grace, M. E., Grabowski, G. A., Aebersold, R., and Withers, S. G. (1994) Identification of Glu340 as the active-site nucleophile in human glucocerebrosidase by use of electrospray tandem mass spectrometry. *J. Biol. Chem. 269*, 10975−10978.
(73) Premkumar, L., Sawkar, A. R., Boldin-Adamsky, S., Toker, L., Silman, I., Kelly, J. W., Futerman, A. H., and Sussman, J. L. (2005) X-ray structure of human acid-β-glucosidase covalently bound to conduritol-B-epoxide. Implications for Gaucher disease. *J. Biol. Chem. 280*, 23815−23819.
(74) Wei, R. R., Hughes, H., Boucher, S., Bird, J. J., Guziewicz, N., Van Patten, S. M., Qiu, H., Pan, C. Q., and Edmunds, T. (2011) X-ray and biochemical analysis of N370S mutant human acid β-glucosidase. *J. Biol. Chem. 286*, 299−308.
(75) Leinekugel, P., Michel, S., Conzelmann, E., and Sandhoff, K. (1992) Quantitative correlation between the residual activity of β-hexosaminidase A and arylsulfatase A and the severity of the resulting lysosomal storage disease. *Hum. Genet. 88*, 513−523.
(76) Desnick, R. J., and Fan, J. Q. (2006) Pharmacologic chaperone therapy for lysosomal diseases. In *Gaucher Disease* (Futerman, A. H., and Zimran, A., Eds.) pp 377−397, CRC Press, Boca Raton, FL.